10th Pacific Symposium on Flow Visualization and Image Processing
Naples, Italy, 15-18 June, 2015

Flow characteristics around a vortex flow meter via CFD and PIV methods

Muammer Ozgoren[1,*], Sercan Yagmur[1], Sercan Dogan[1], Muharrem H. Aksoy[1], Eyub Canli[1], Ilker Goktepeli[1]

[1]Department of Mechanical Engineering, University of Selcuk, Konya, Turkey
*corresponding author: mozgoren@selcuk.edu.tr

Abstract Vortex flow meters play important role for flow rate measurements of liquids and gases. These devices provide high precision, accuracy, repeatability, low maintenance requirement and their measurements are independent of the construction material properties as well as Reynolds number. Due to its insensitiveness of most parameters of the fluid including density, temperature and pressure, the vortex flow meter is considered as a potential solution to the flow measurement in a wide aplication area. Working principle of the vortex flow meters is based on the measurement of vortex shedding frequency of the Karman Vortex streets in the wake region of the bluff body such as a triangular cross-section. In this study, vortex shedding frequency and flow characteristics such as instantaneous and time-averaged vector fields, streamline topology, vorticity, velocity component contours and root mean square (rms) variation depending on the Reynolds numbers at Reynolds number 5800 and 11600 were investigated by means of time-resolved Particle Image Velocimetry (PIV) and Computational Fluid Dynamics (CFD) with three different Turbulence Models. The sharp-tip corner of the triangle cross-section cylinder is exposed to the free stream flow while the other two sharp-edge corners are placed to the downstream side to form powerful, stable and continuous vortex shedding.The experimental studies are performed in an open water channel at Selcuk University of Advanced Technology Research and Application Center in Konya, Turkey. The experimental results are compared to the numerical results obtained by transient simulations with RANS (k-ε and k-ω methods) and Large Eddy Simulation (LES) turbulence models using ANSYS-Fluent Software. It is seen that the RANS method does not give comparable results with the PIV when compared to the LES method for the flow structure and drag coefficients. On the other hand, it is seen that the results of k-ε and k-ω methods are very close. The LES turbulence method and experimental results have a good agreement. For instance, at Re=11600, the Strouhal numbers from PIV and LES analysis are found to be 0.228, which yields close agreement with literature value of 0.250. In the literature, LES method is also suggested for the simulation analysis of vortex shedding dominant flow as it is demonstrated in this study even though LES analysis requires more iteration time due to the increased mesh size and corresponding equation numbers. In addition, drag coefficient was also numerically calculated. It is shown that the wake length in x and y directions and size of the foci of the streamlines are decreasing by increasing Reynolds numbers in time-averaged flow patterns from both CFD and PIV. The time averaged vector fields, streamline topology, vorticity and velocity component contours have considerable symmetry with respect to a line passing through the sharp-tip corner of the triangle cross-section cylinder. Contours of the time-averaged streamwise velocity results at Re=11600 display that the stagnation point around the symmetry plane moves further upstream with respect to the Re=5800.

Keywords: CFD, PIV, Strouhal number, turbulence, vortex flow meters, vortex shedding, vorticity

1. Introduction

The fluid flow around bluff bodies (e.g., circular, square, rectangular, triangle cross-sectional cylinders) has been investigated by researchers for centuries because of its importance in various engineering applications, such as electronic cooling, heat exchanger systems, bridge piers, high-rise buildings and flow dividers, sensors and probes etc. [1]. Another important industrial application area is the design of vortex flow meters which is expressed as a good choice for flow measurements. The main working principle of these devices are the measurement of vortex shedding frequency in the wake region of bluff bodies assuming that Strouhal number keeps constant for Reynolds numbers . This vortex trail in the wake region of the bluff body is called Von Karman Vortex Street. If the Reynolds number is not too small the flow is inherently unsteady and a Karman Vortex Street appears with a well-defined frequency. If the Reynolds number is sufficiently high, the flow will be turbulent and a turbulence model must be included the turbulent fluctuations [2].

Many experimental and numerical investigations of flow past bluff body have been performed so far, because cylinder-like structures are commonly used in many applications. In spite of such wide applications, limited information is available in the open literature; most research in this field is related to the circular and square cross-sectional cylinders. Ozgoren focused on the generation of vertical structures of the near-wake region appearing from flow passing the different cross sectional cylinders for $550 \leq Re \leq 3400$ in order to explain the physics of the flow structure. He concluded the Strouhal number, as well as the wake patterns, are functions of the cross-section of the cylinders and Reynolds numbers [3]. Okajima carried out an experimental study of flow past the square cylinder as well as the rectangular cylinder for $70 \leq Re \leq 20000$ to determine the vortex shedding frequencies. The results showed that there was an abrupt change in Strouhal number when the aspect ratio of the cylinder was reduced to the range 2–3. Strouhal numbers for the square cylinder with an increasing angle of incidence from 0˚ to 45˚ were examined using a hot-wire probe in a closed circuit wind-tunnel and maximum St number was occurred as 0.13 [4].

Vortex shedding studies are not limited for only circular cross-sectional cylinder. One of such study, flow structure around a single sphere and three spheres in an equilateral-triangular arrangement by PIV was performed by Ozgoren and dye visualization technique in an open water channel. Three spheres were varied in the range of different gap ratios. He concluded that because of the interference of the shedding shear layers and the wakes, the wake region of the two downstream spheres behind the leading sphere was more complicated. It was also observed that a continuous flow development involving shearing phenomena and the interactions of shedding vortices caused a high rate of fluctuations over the whole flow field [5]. Wei-Xi and Hyung studied numerically on vortex shedding from a circular cylinder near a moving wall. A gap ratio between the moving wall and the circular cylinder is described by using instability theory. The drag, lift and pressure coefficients were submitted as a function of the gap ratio, and Strouhal number was also discussed [6]. Hatef and Anderson examined unsteady vortex shedding from a hexagonal cylinder for three different Reynolds numbers and two different orientations of the cylinder, numerically. They identified that the orientations of cylinder was the function of Strouhal number, and it is higher than a face-oriented cylinder, behind a corner-oriented cylinder. The results were compared with previous findings for a square cylinder; They found that higher Strouhal number when corner of the square exposed to the free stream than with face orientation was obtained [7]. Knauss et al. measured the vortex shedding frequency in the wake of elliptical and square cylinders. They expressed that the Strouhal number should be based on the height of the projected cylinder on a plane normal to the flow direction rather than on a geometrical measurement of the bluff body. It was pointed out that the shedding frequency was almost unaffected by Reynolds number [8].

Liu et al. was investigated the flow characteristics around different cross-sectional study. They studied the wake characteristics of a square cylinder in proximity to a plane wall for two different gap distances to width ratio, i.e. G/D=0.25 and 0.5. For the measurements of velocity and pressure fluctuations hot-wire anemometer and split-fiber film methods were used. They concluded that at the gap ratio of G/D=0.5, the dimensionless vortex shedding was found as St=0.13 by inspection of the stream wise velocity spectra and it was reduced to St=0.116 at G/D=0.25 [9]. Shun and Chen presented the flow patterns and vortex shedding behavior around a square cylinder at different incidence angles by PIV. The surface-pressure profile, drag coefficient, lift coefficient and vortex-shedding frequency were determined using a pressure transducer and hot wire anemometer data. The results were showed that the lift coefficient did not significantly vary with Re. The minimum drag coefficient (C_D) value occurred at θ=12˚, while the highest lift coefficient (C_L) occurred at θ=13˚. At θ=0˚, they obtained that the relationship between St and Re was St=0.13-36.83/Re. The minimum St number was calculated at $\theta=0^o$ while the maximum was determined at θ=15˚[10]. Another similar study was studied by Bouris and Bergeles. They numerically analyzed the vortex shedding from a square cylinder by 2D LES method. They found that St=0.134 and C_D= 2.18 at Re=22000 and compared numerical analyses findings with both literature and their previous experimental results. They yielded well agreement and obtained that the differences were nearly 1.5% for Strouhal number and 4% for drag coefficient [11]. Flow structures around the square cylinder positioned at different angles from 0˚ to 45˚ and their influence on the wake properties were studied by Huang et al. Surface-oil flow method was used for flow topology at Reynolds numbers between $3.9x10^4$ and $9.4x10^4$. The Strouhal number and turbulence in the wake region were varied for different incidence angle. At the critical incidence angle of 15˚, the Strouhal number reached a maximum of 0.2 and with the reducing incidence angle, the wake length was getting a minimum value, and a minimum drag coefficient [12].

Vortex shedding was also investigated by using active and passive flow control methods by some of the researchers. Gu et. al applied a passive control of flow structure for a cylinder in which they investigated experimentally flow characteristics of a circular cylinder with attached rotatable splitter plate at different angle with ratios of length to the cylinder diameter (L/D) from 0.5 to 6.0, in a range of Reynolds numbers from $3x10^4$ to $6x10^4$ by using smoke visualization technique. The shedding frequency is higher than bare cylinder for L/D=2 but it becomes lower than that for L/D=4.2. The St number decreases from 0.226 to 0.148 with increasing L/D values from 0.5 to 3.5. Due to the different equilibrium situation, St rises up to about 0.17 suddenly between L/D=3.5 and 4.0, and a second peak frequency appears [13]. Sang and Jung investigated the wake behind a circular cylinder by applying a rotational oscillatory motion. They stated that the rotational oscillatory motion of the cylinder declined the length of the vortex formation region and enhanced the mutual interaction between large-scale vortices across the wake centerline [14]. Lam investigated the wake characteristics behind the steady rotating cylinder in the range of Re=3600-5800 and circumferential speed at the cylinder surface normalized by the free-stream velocity value between 0 and α=2.5. It was observed that for the rotation speeds lower than α=1.9, vortex shedding was seen clearly by PIV measurements system. The vortex shedding frequency was found to increase with the cylinder rotation speed. The Strouhal number increased slowly from St=0.175 to 0.23 when α raised from 0 to 1. With the increasing α, the vortex formation length was observed to reduce [15]. Kalmbach and Breuer investigated the fluid structure around the flexible plate mounted cylinder at Re=30470 by using PIV and V3V (volumetric three-component velocimetry) method. They determined the Strouhal number as St=0.177 where the oscillation frequency of cylinder is 11.2Hz. In addition, they also obtained lift and drag coefficients by using data displacement PIV-based force measurements. They concluded that this method is the new technique of analyzing flow structure and it can be coupled with the CFD results [16].

There are limited studies that focus on a flow around triangular cylinder. One of the examples of this subject was performed by Xing and Perot. They simulated the flow around the triangle cylinder to analyze flow field, time-averaged velocity profile and Strouhal number by using turbulent body force potential model. They obtained that numerical simulation results were well agreement with experimental results, and the feature that this model conserves kinetic energy intensity both globally and locally makes it a good selection for performing turbulence model [2]. The vortex shedding frequency, drag coefficient, pressure coefficient and streamline topology were analyzed for the flow around a square, trapezoid and triangle cylinders by Cheng and Liu at Re=250 [17]. Two dimensional numerical results indicated that the vortex shedding frequency was peaked at the trapezoid cross sectional cylinder and Strouhal number was occurred as St=0.154 for this geometry. Strouhal number was nearly 0.135 and 0.145 for triangle and square cylinders, respectively. In addition, drag coefficient was decreased from triangle to square cylinder and it was C_D=2.3 for triangle cylinder, C_D=2.1 and 1.8 for trapezoid and square cylinder [17]. Dhiman and Syham examined the Reynolds number effect on the unsteady heat transfer around an equilateral triangular cylinder to find out Nusselt numbers at the range of Re=50 to 150. They also investigated the variation of Strouhal number and the drag coefficient. Such at Re=50, Strouhal number and drag coefficient were obtained as 0.145 and 1.54, respectively [18].

On the other hand, sufficient information is available in the literature on the flow around a triangular cylinder in the turbulent flow regime (Saad [19]; Nakagawa [20]; Tatsuno et al. [21]; Wahed et al. [22]; Sharif and Gu [23]; Camarri et al. [24]; Chattopadhyay [25]; Peng et al. [26]; Srigrarom and Koh [27]; Dmitry et al.[28]; Hasse et al. [29]; Johansson et al. [30]; Sjunnesson et al. [31]; Srikant et al. [32] ; De and Delal [33]; Turner et al. [34]; Zeitoun et al. [35] and Stefan et al. [36])

The fluid flow characteristics around a triangular cylinder are investigated only by a few researchers. This has motivated us to examine the flow across an equilateral triangular cross-section cylinder in a steady flow regime. The propose of this study is to determine vortex shedding frequency and flow characteristics around an equilateral triangular cylinder such as instantaneous and time-averaged vector field, streamline topology, vorticity, velocity component contours and root mean square (rms) variation depending on the Reynolds numbers at Re=5800 and Re=11600 by means of time-resolved PIV and three different CFD turbulence models.

2. Methods

2.1. Experimental Setup

Experiments were carried out in the recirculating open water channel with the rectangular test section of 0.77m (width) x 0.60m (height) x 6.00m (length) in the facilities of Advanced Technology Research and Application Center of Selcuk University in Turkey shown schematically in Figure 1. The walls of the test-section were made of 15 mm thick transparent acrylic and glass plates to facilitate laser transmission and flow visualization. A centrifugal pump was used to circulate the water in the channel and before the water reaching settling chamber, a contraction section and a honeycomb were mounted in sequence to provide flow homogeneity. The speed of fluid in the test-section was controlled from 116 to 232 mm/s by a frequency converter of the pump, the Reynolds numbers range at Re=5800 to 11600 based on the characteristic length of the equilateral triangle geometry having a 50 mm edge. The cylinder height is 0.6m. The uncertainty of free-stream turbulence intensity was less than 1%. The equilateral triangular cylinder model was placed horizontally in uniform flow condition of the water tunnel. The sharp-edge of the triangle is positioned in the opposite direction to the flow. The cylinder was made of acrylic material with the 5mm thickness and the surface was highly polished to avoid the effects of surface roughness for better optical effects.

As a light sources, Nd:YAG laser which was located vertically from the channel bottom was used to generate a laser sheet that was perpendicular to the axis of the cylinder was passed through them with 1000 pulse per second, and the suitable combination of cylindrical lenses was combined to the compact laser to produce a 1-mm-thick light sheet along the mid-point of the cylinder. An ensemble of 3700 image pairs was taken for all measurements by a CMOS camera with a resolution of 1632 x 1200 pixels.

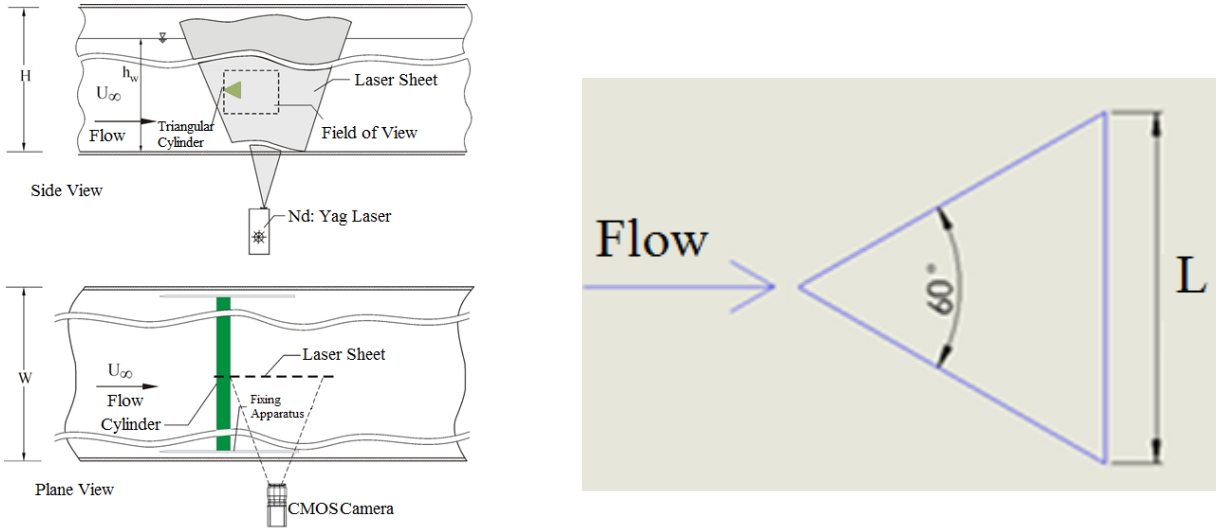

Fig. 1 Schematic view of the PIV system experimental setup, laser illumination for a triangular cylinder located in a uniform flow condition.

Adaptive correlations with an interrogation window of 32 x 32 pixels in the image were selected and converted to approximately 2.0 x 2.0 mm^2 grid size consisting of 7400 (100 x 74) velocity vectors. During the cross-correlation step an overlap of 50% and window deformation were used to all interrogation areas in order to satisfy the Nyquist criterion. For the flow visualization, with the close enough densities to the water, in 10 μm diameter silver coated hollow glass spheres was added to the water. Additionally, the high-image-density criterion was contented by ensuring that a minimum of approximately 20–30 particles was contained within the interrogation area. Dantec Dynamic Studio software employing the adaptive correlation algorithm including proper filters was used for computing the raw displacement vector field from the particle image data.

2.2. Numerical Study

For the numerical investigations, the turbulent viscosity is computed in many ways in the literature. In this study, three different turbulence methods were used to simulate the flow field around the triangular cylinder. The first approach used the k-ε turbulence model, which has turbulent kinetic energy (k) and rate of dissipation of turbulent kinetic energy (ε). The second one is the k-ω turbulence model approach, k is the transport equation for turbulent kinetic energy, and ω is the turbulent specific dissipation. The final turbulence model was based on a large eddy simulation (LES), which analyzes most of the turbulent length scales. The governing equations for an incompressible flow form of the continuity equation and the Reynolds Averaged Navier-Stokes are specified below in the following equation [40]:

$$\frac{\partial \overline{u_i}}{\partial x_i} = 0 \tag{1}$$

$$\frac{\partial \overline{u_i}}{\partial t} + \frac{\partial \overline{u_i}\overline{u_j}}{\partial x_j} = \frac{1}{p}\frac{\partial \bar{p}}{\partial x_i} - \frac{\partial \tau_{ij}}{\partial x_j} + v\frac{\partial^2 \overline{u_i}}{\partial x_i \partial x_j} \tag{2}$$

where u_i are the filtered velocity components along the Cartesian coordinates x_i, p is the pressure, q is the fluid density and v is the kinematic viscosity of the fluid.

2.2.1 *k-ε* turbulence model

The model transport equation for k is derived from the exact equation, while the model transport equation for ε was obtained using physical reasoning and bears little resemblance to its mathematically exact counterpart. Lun et. al. used this model in their study [37, 40]. The turbulence kinetic energy, k, and its rate of dissipation, ε, are obtained from the following transport equations:

$$\frac{\partial}{\partial t}(\rho k) + \frac{\partial}{\partial x_j}(\rho k u_i) = \frac{\partial}{\partial x_j}\left[\left(\mu + \frac{\mu_t}{\sigma_k}\right)\frac{\partial k}{\partial x_j}\right] + G_k + G_b - \rho\varepsilon - Y_M + S_k \tag{3}$$

$$\frac{\partial}{\partial t}(\rho \varepsilon) + \frac{\partial}{\partial x_j}(\rho \varepsilon u_i) = \frac{\partial}{\partial x_j}\left[\left(\mu + \frac{\mu_t}{\sigma_\varepsilon}\right)\frac{\partial \varepsilon}{\partial x_j}\right] + G_{1\varepsilon}\frac{\varepsilon}{k}(G_k + G_{3\varepsilon}G_b) - G_{2\varepsilon}\rho\frac{\varepsilon^2}{k} + S_\varepsilon \tag{4}$$

In these equations, G_k represents the generation of turbulence kinetic energy due to the mean velocity gradients, G_b is the generation of turbulence kinetic energy due to buoyancy, YM represents the contribution of the fluctuating dilatation in compressible turbulence to the overall dissipation rate, C_1, C_2, and C_3 are constants. σ_k and σ_ε are the turbulent Prandtl numbers for k and ε, respectively. S_k and S_ε are user-defined source terms [40].

2.2.2 *k-ω* turbulence model

The standard k-ω model is an empirical model based on model transport equations for the turbulence kinetic energy (k) and the specific dissipation rate (ω), which can also be thought as the ratio of k. As the k-ω model has been modified over the years, production terms have been added to both the k and ω equations, which have improved the accuracy of the model for predicting free shear flows. Shome benefited from this method in his study [38, 40].

$$\frac{\partial}{\partial t}(\rho k) + \frac{\partial}{\partial x_j}(\rho k u_i) = \frac{\partial}{\partial x_j}\left[\left(\mu + \frac{\mu_t}{\sigma_k}\right)\frac{\partial k}{\partial x_j}\right] + G_k - Y_k + S_k \tag{5}$$

$$\frac{\partial}{\partial t}(\rho\omega) + \frac{\partial}{\partial x_j}(\rho\omega u_i) = \frac{\partial}{\partial x_j}\left[\left(\mu + \frac{\mu_t}{\sigma_k}\right)\frac{\partial \omega}{\partial x_j}\right] + G_\omega - Y_\omega + S_\omega \quad (6)$$

In these equations, G_k represents the generation of turbulence kinetic energy due to mean velocity gradients. G_ω represents the generation of ω. Γ_k and Γ_ω represent the effective diffusivity of k and ω, respectively. Y_k and Y_ω represent the dissipation of k and ω due to turbulence. All of the above terms are calculated as described below. S_k and S_ω are user-defined source terms [40].

2.2.3. The Large Eddy Simulation (LES) Model

The fundamental principal operation in large eddy simulation is low-pass filtering. This operation is applied to the Navier–Stokes equations to eliminate small scales of the solution. The mean flow and all the large eddies are modeled in LES and the remaining small eddies are computationally determined in a parametric function. In order to distinguish between the large scales and small scales, a filter function is used in LES. From equation (2), applying the filtering operation, the incompressible Navier–Stokes equations for the evolution of the large-scale motions is obtained [40]. Kim et. al. used this turbulence model in their study [39]. The influence of the small scales on the large (resolved) scales takes place through the subgrid scale stress tensor as followed by:

$$\tau_{ij} = \overline{u_i u_j} - \bar{u}_i \bar{u}_j \quad (7)$$

resulting from the filtering operation, which are unknown and must be modeled with a subgrid model which is based on the eddy viscosity approach:

$$\tau_{ij} - \frac{1}{3}\tau_{kk}\delta_{ij} = -2\mu_t \bar{S}_{ij} \quad (8)$$

where the trace of the subgrid scale stresses τ_{kk} is incorporated in the pressure resulting in a modified pressure term,$\mu_t$is the subgrid-scale viscosity, and $\bar{S}_{ij}$ is the resolved scale of the strain rate tensor and defined by:

$$\bar{S}_{ij} = \frac{1}{2}\left(\frac{\partial \bar{u}_i}{\partial x_j} + \frac{\partial \bar{u}_j}{\partial x_i}\right) \quad (9)$$

The fundamental and most well-known subgrid scale models were recommended by Smagorinsky and later by Lilly. In the both of their model, the eddy viscosity as:

$$\mu_t = \rho l_s^2 \left|\bar{S}_{ij}\right| \quad (10)$$

in that equation l_s is the length of mixing for the subgrid scales and when the resolved scale of the strain rate tensor defined by:

$$\left|\bar{S}_{ij}\right| = \sqrt{\bar{S}_{ij}\bar{S}_{ji}}\, l_s \quad (11)$$

It can be used to compute as:

$$l_s = \min\left(Ky, C_s V^{1/3}\right) \quad (12)$$

where *K* is the von Karman constant, *y* is the interval to the closest wall, C_s is the Smagorinsky constant, and *V* is the computational cell volume[40].

2.2.4 Computational domain and solution setup

In the present study, numerical analyses have been simulated at low flow Reynolds number tested in water channel with three different turbulence models. A commercial software with finite volume method, named ANSYS-FLUENT, has been used [40]. Flow domain was prepared as showed in Figure 2 and the triangular cylinder was located at the origin of coordinate system. The inlet of the flow domain was started 4.0L far away from the tip of the triangle to the outlet about 16.0L. L, an edge of the triangular cylinder, is the characteristic length for the triangular cylinder. From the mid plane of the flow volume, height and width were 9.0L and 12.0L, respectively.

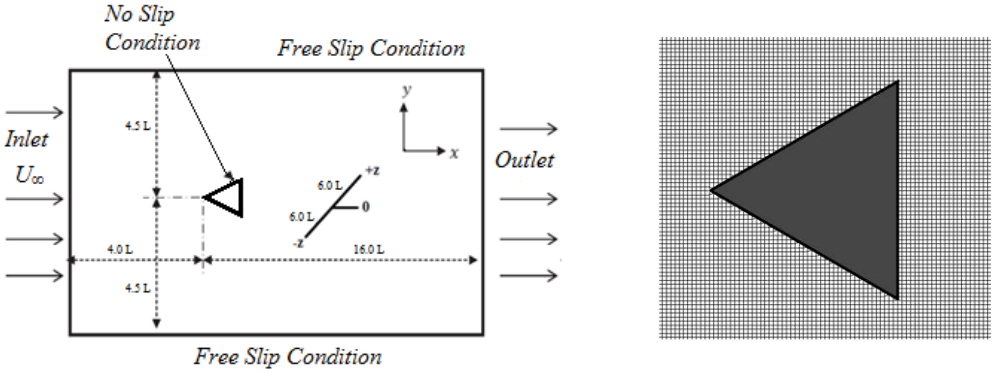

Fig. 2 Flow domain and the grid structure on the x-y plane

The flow domain was divided into three parts and a number of unstructured cut-cell grids was used to analyze flow field. From separated parts, the mesh was created denser at the closer region of triangular cylinder and in the boundary layer. Figure 2b shows the grid on the x–y plane and it is also uniform along the z direction. To receive a better results and view detailed vortex structures, the grid size of the flow domain is $10x10^6$ for the finer grid number in the all fluid domain, which provides enough mesh size to simulate the experimental flow volume of the PIV. Mesh independence study was also done with coarsen and fined grid size considering the variation of the drag coefficient (C_D) of triangular cylinder with respect to the grid size for three turbulence models (LES, k-ε and k-ω) in Table 1 at Re=11600.

Table 1 Grid independence study for drag coefficient (C_D) of triangular cylinder at Re=11600

	C_D		
Grid Size	LES	k-ε	k-ω
2.500.000	1.582	1.458	1.483
5.000.000	1.518	1.275	1.256
10.000.000	1.443	1.149	1.138
18.000.000	1.43	1.138	1.136

As seen in Table 1, the C_D changes with the grid size and the difference is about 2% when the values of grid size increase from 10 million to 18 million. For low grid size of flow domain, percentage of difference between the C_D values is high and for transient analyses and it is hard to capture vortex shedding. Therefore, 10 million grid size of flow domain was used to analyses flow field, grid size effect on the C_D was small enough and it requires less computer capacity than 18 million one. As shown in Figure 1, velocity inlet was used for the inlet boundary conditions with the uniform water flow and pressure outlet was used for the outlet boundary conditions with the atmospheric operating pressure. Because of the no slip boundary condition, a wall function was defined where the model was contacted to the water. To be not affected by the wall function, the top and side surfaces of the flow volume were described as free slip condition. These boundary conditions were provided as standard for all turbulence models.

3. Results and Discussion

In this section, some of the experimental and CFD results are presented and discussed comparatively. Flow patterns of the normalized time-averaged vector field (<V>), stream-wise velocity contour (<u*>), cross stream velocity (<v*>), standard deviation distribution of streamwise velocity component ($<\sigma_u>$), standard deviation distribution of cross stream velocity ($<\sigma_v>$), vorticity structures (<ω*>), streamline topology (< ψ >) components of experimental and numerical analysis (LES, k-ε and k-ω) results for a triangular cross-sectional cylinder are presented in Fig. 3 and Fig. 4 at Re=5800 and Re = 11600, respectively. The full range of conditions was expected in the case of a triangular cylinder in a uniform flow for experimental and numerical calculations. All figure dimensions are normalized with the appearance characteristics length as x/D. Here, D is equal to L in Figure 1. The negative and positive contour values were indicated with the dashed and solid line, respectively.

The stream-wise velocity contours (<u*>) in Figs 3 and 4 display that both positive and negative velocity contours are occurred for each Reynolds number. Substantial regions of negative (reverse) flow are evident and it is also possible to define the location of a stagnation point in which velocity contour value is zero. The values of the maximum positive velocity contours were found to be 0.16 for experimental results at Re=5800 and 0.3 for both experimental and k-ε turbulence model results at Re=11600. On the other hand, the values of the maximum negative velocity contours were -0.04 for experimental and k-ω turbulence model results at Re=5800 and also -0.12 for LES turbulence model results when Re=11600. The lower velocity contours values were seen at the central location and around the symmetry axis of the triangular cylinder for all results. When the cross stream-wise velocity contours were examined, two velocity contours with a mirror appearance that are existed both upper and lower the symmetry axis of the triangular cylinder in the downstream. The LES turbulence model yields closer flow field appearance than the k-ε and k-ω models for negative and positive contours for both Reynolds numbers.

The patterns of cross-stream velocity are detectable near the interface between the separating shear layers as shown in third row of Figs 3 and 4. The contours of constant cross-stream velocity (<v*>), close to the base of the cylinder and backward corner of the body have relatively larger values. A large amplitude of cross-stream velocity for both Re numbers might indicate that the developing shear layers which originally separate from the cylinder entrained a significant mass flow in the base region through both sides of the cylinder. Same-signed cross-stream velocity components extend one side of the centerline to the other for all results.

Patterns of time-averaged streamline topology (< ψ >) identify the major changes of the near-wake behind the cylinder. They exhibit well-defined critical points, e.g. foci (centers of vortices) designated as F_1 and F_2 and saddle points (apparent intersections of streamlines) denoted as S, as shown in the bottom row of Figs. 3 and 4.Streamline topologies were shown that the wake region length at Re=5800 is longer than Re=11600 and the stagnation point approached to the trailing edge with the increasing Reynolds numbers as seen from time-averaged experimental and all numerical turbulence models.. From experimental results, two symmetrical foci were formed at the trailing edge with the length of $1.8 < x/L < 1.9$ and $1.6 < x/L < 1.7$ at Re = 5800 and 11600, respectively. When the numerical results with the experimental results were compared, the method using LES turbulence model gave the more similar flow field than k-ε and k-ω for both Reynolds numbers. In the x-direction, the length of the foci was longer at k-ω turbulence model than the other turbulence models and experimental study for both Reynolds numbers. However, in the y direction, the length of foci was the largest at Re=5800 for k-ε turbulence model. Furthermore, the length of the wake region was narrower for experimental results when they were compared with all numerical models. However, the difference of the wake size between experimental and CFD was negligible on the conditions of LES turbulence model.

Experimental and LES turbulence model results show similar vorticity structure for Re=5800 and 11600. Nevertheless, the vorticity contours results of k-ε and k-ω turbulence models are slightly different. The downstream length of the contours at both Re = 5800 and 11600 was longer for k-epsilon and k-omega turbulence models than the LES and experimental results. For all results, positive and negative contours have

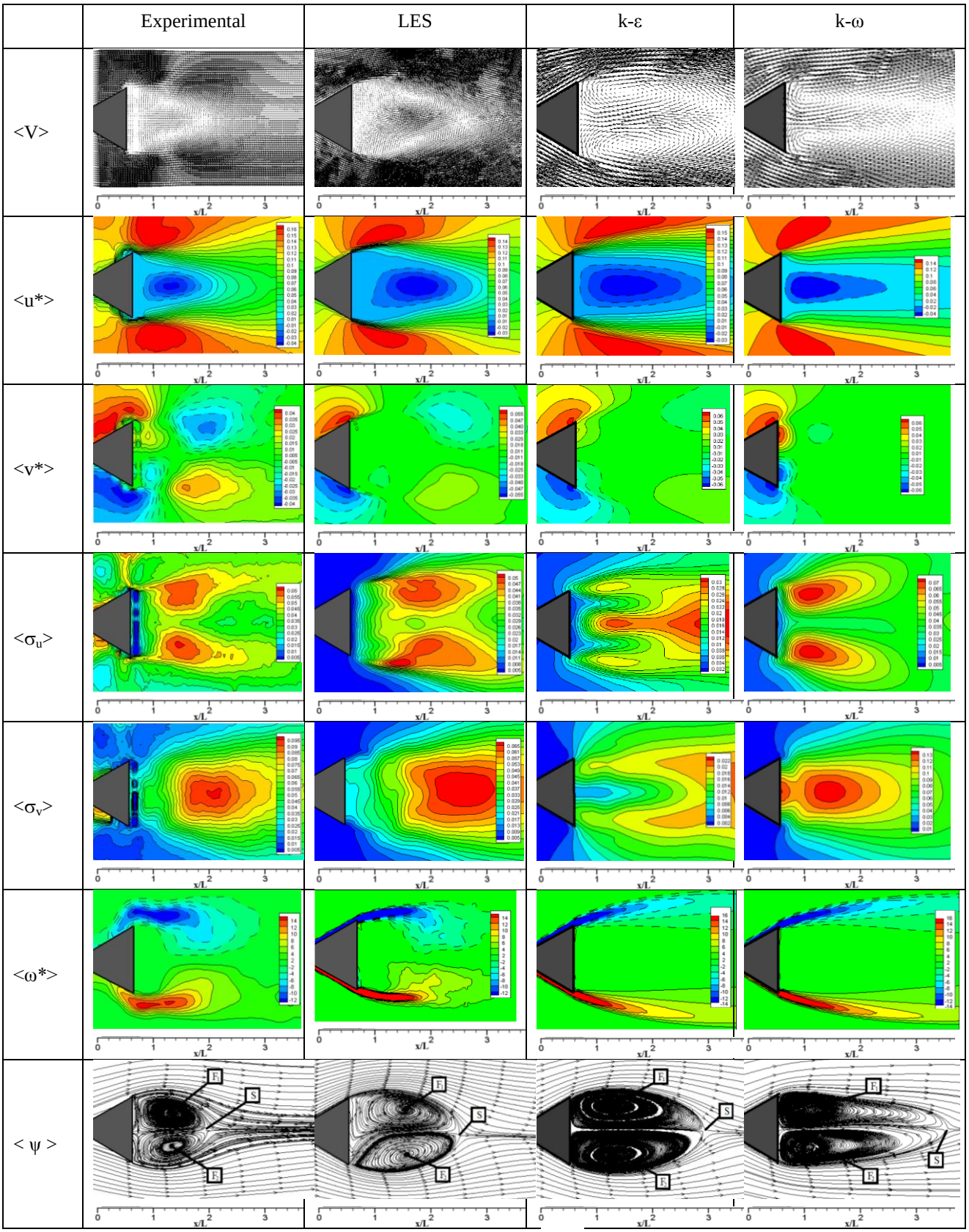

Fig 3. Flow patterns of the normalized time-averaged vector field (<V>), stream-wise velocity contour (<u*>), cross stream velocity (<v*>), standard deviation distribution of streamwise velocity component (<σ_u>), standard deviation distribution of cross stream velocity (<σ_v>), vorticity structures (<ω*>), streamline topology (< ψ >) components of experimental and numerical analysis (LES, k-ε and k-ω) results at Re = 5800 for a triangular cross-sectional cylinder.

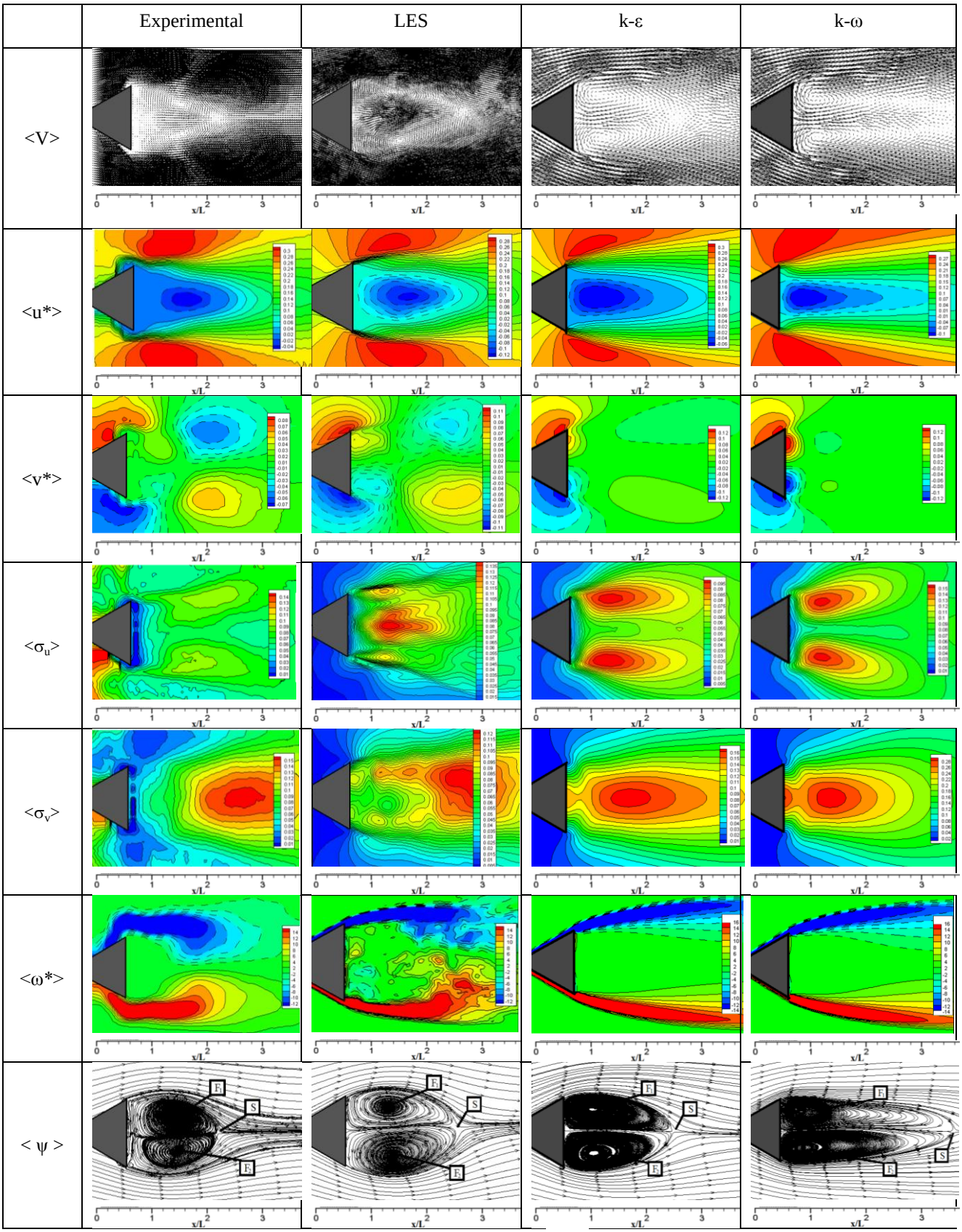

Fig 4. Flow patterns of the normalized time-averaged vector field (<V>), stream-wise velocity contour (<u*>), cross stream velocity (<v*>), standard deviation distribution of streamwise velocity component (<σ_u>), standard deviation distribution of cross stream velocity (<σ_v>), vorticity structures (<ω*>), streamline topology (< ψ >) components of experimental and numerical analysis (LES, k-ε and k-ω) results at Re = 11600 for a triangular cross-sectional cylinder.

symmetrical values with respect to the symmetry axis of the geometry. Two symmetrical time-averaged vortices were occurred around the bluff bodies, one was counter clockwise direction while the other was in the opposite direction. Generally, at high Reynolds numbers, the length of vorticity is smaller for all flow patterns, higher values of vorticity contours cover a wider area and thus the flow is more chaotic. There were similarities between stream-wise velocity, normal velocity component, rms (root mean square) of velocity components in x and y-axes in experimental study and LES turbulence model. The similarity between experimental results and LES turbulence models were demonstrated by the shapes of stream-wise and counter stream-wise velocity contours. Overall comparison of the turbulence model results shows that similarity between k-ε and k-ω turbulence models are more suitable when it is compared with LES turbulence model. In the base region, two separated shear layers with oppositely signed vortices interact more directly and vigorously, resulting in substantial cancellation of the averaged vorticity (<ω*>), as seen in Figs. 3 and 4. The dominant vortex shedding frequency f is determined from power spectra of recorded DPIV data in the near wake region of the cylinders, particularly inside the free shear layer region, at the various selected points. Statistical characteristics of the instantaneous streamwise velocities in time series are determined in order to get information in the frequency domain by using spectral analysis, i.e. Fast Fourier Transformation (FFT) [3]. In addition, Strouhal number (St), pressure coefficients (C_p) and drag coefficients (C_D) were investigated numerically. However, as there are no force and pressure measurement systems in experimental setup, the pressure and drag coefficients were obtained only with numerical analysis. It can be interpreted that the results are trustable due to the obtained similar flow structures in Figs 3 and 4. Strouhal number can be found as a function of frequency (f), characteristic length (L) and uniform velocity (U_∞);

$$St = \frac{f\,L}{U_\infty} \tag{13}$$

As seen in Figure 5, Power Spectrum - Frequency Curve were drawn with the values of instantaneous streamwise velocity which were taken from sampling point in the wake region. From this curve, the peak point of frequency that shows the dominant vortex shedding frequency was used to calculate Strouhal number. This process was applied for all experimental and numerical analyses.

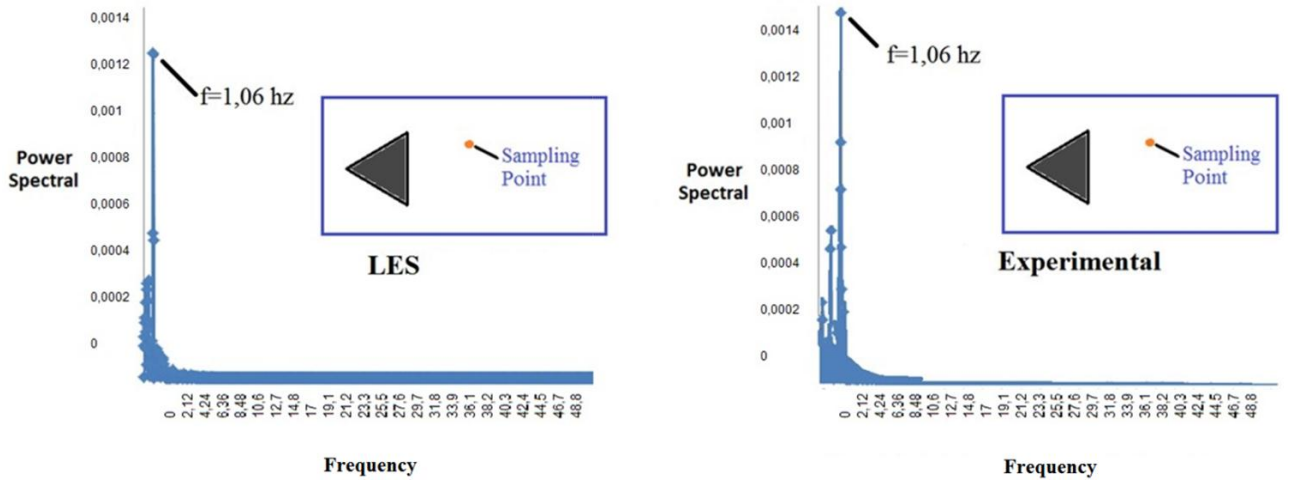

Fig.5 Variation of experimental (right image) and LES model (left image) of Power spectrum against Frequency at Re=11600

In Figure 6, the change of pressure coefficient around the triangular cylinder with LES, k-ε and k-ω models are indicated with respect to xy-plane at Re=5800 and 11600, numerically. The pressure coefficient is defined as;

$$C_p = \frac{P - P_\infty}{\frac{1}{2}\rho {U_\infty}^2} \tag{14}$$

where P is static pressure at the wall, P_∞ is the pressure of oncoming flow, ρ is fluid density and U_∞ is the uniform velocity.

Three different turbulence models were investigated but the results that were established in the k-ε and k-ω were approximately overlapped. On the other hand, the results of the LES turbulence model were partially different. As seen clearly in Figure 6, C_p was the maximum at the stagnation point A since the velocity value of the fluid flow was equal to zero. From leading edges to trailing edge, the pressure coefficients decreased at both Reynolds numbers of all turbulence models. The C_p valuses becomes zero approximately 0.82L for the k-ε and k-ω models and 0.73L for the LES model along the edge AC and AB. At the trailing edge, the pressure coefficients take negative values due to the reversed flow that is occurred in the wake region. At the point that pressure coefficient C_p equaled to the zero, the flow separation observed. Figure 6 also indicated that flow separation which occurred around the triangular cylinder. According to this condition when approaching from corner A to the corner B of the triangular cylinder, flow separation is occurred at a point that was very near to B corner. In addition, in the edge of the triangular cylinder from corner A to corner C, flow separation was seen at a point that was very close to the corner C. Stagnation point occurred as expected between A and B points and was also seen symmetrically between A and C. As shown in Fig. 6, C_p was remained stable between B and C points where it has negative values. When all turbulence models are compared, it is clearly seen that C_p values of k-ε and k-ω turbulence models were overlapped but LES turbulence model showed a different distribution for C_p values where between B and C points. Tatsuno et al. and Dmitry et al. also obtained the pressure coefficients experimentally at Re=90000 and numerically at Re=45000, respectively [21-28]. Present results gave well agreement between those numerical and experimental results.

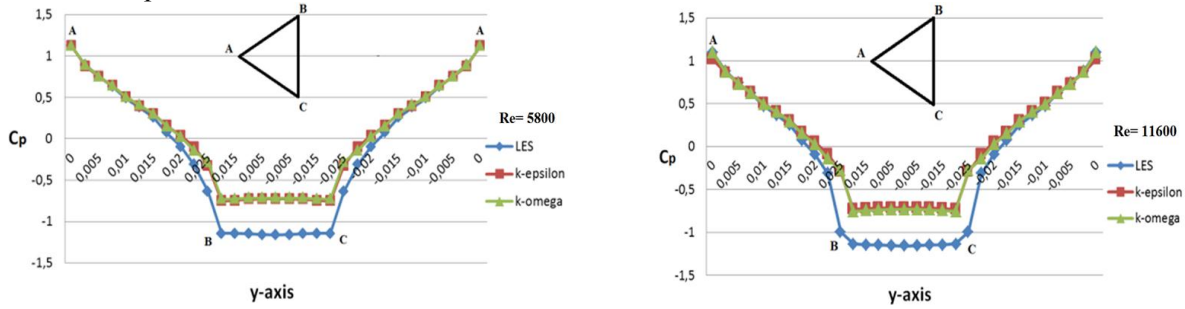

Fig.6 Pressure coefficient value at Re=5800 and Re=11600 for LES, k-ε and k-ω models

The drag coefficient is described as follows:

$$C_D = \frac{2F_d}{\rho {U_\infty}^2 A} \tag{15}$$

where: F_D is the drag force in the free stream flow direction of the velocity and A is the projection area of the front view. In Figure 7, the time-averaged and instantaneous drag coefficient by using LES method for the circular cylinder at Re=11600 is given. After providing uniform flow conditions, considering experimental time-step, which is 0.0016 s with 3700 step, LES was used numerical analysis and the average drag coefficient was found to be C_D=1.44. This result was almost overlapped with Stefan [22]. Mean drag coefficient results of LES, k-ε and k-ω model for both Reynolds numbers are presented in Table 2.

In Table 2, Strouhal numbers from experimental results were found to be 0.217 and 0,228 at Re=5800 and Re=11600, respectively. The closest numerical results to the experiments were provided with St=0.216 and 0.228 in LES turbulence model of Re=5800 and 11600. The values that were achieved in k-ε and k-ω turbulence models were different from LES turbulence model and experimental results whereas those were nearly same in k-ε and k-ω turbulence models and it was around St=0.23 at both Reynolds numbers. Numerical and experimental results were also compared with literature and the results of present study were similar to them.

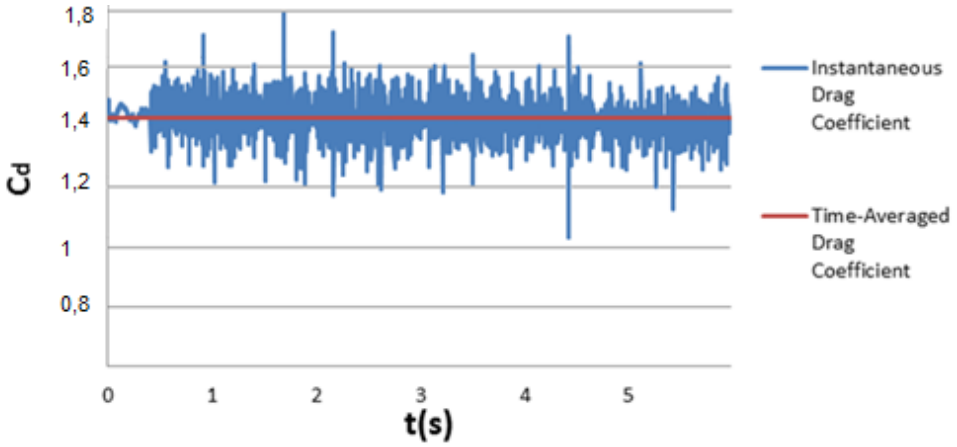

Fig.7 Variation of drag coefficient with LES method for the equilateral triangular cylinder at Re=11600

Table 2 Comparison of Strouhal number and drag coefficient for a triangular cylinder

	St	C_D
LES (Re=5800, present)	0.216	1.467
k-omega (Re=5800, present)	0.228	1.140
k-epsilon (Re=5800, present)	0.236	1.179
Experimental (Re=5800, present)	0.217	-
LES (Re=11600, present)	0.228	1.441
k-omega (Re=11600, present)	0.233	1.131
k-epsilon (Re=11600, present)	0.241	1.141
Experimental (Re=11600, present)	0.228	-
Xing and Blair [2] (Re=45800)	0.250	-
Stefan et. al.[36] (Re=58000)	0.270	1.390
Dmitry et al. [28] (Re=45000)	0.280	-
Hasse et al. [29] (Re=45000)	0.250	-
Sjunnesson et al. [31] (Re=45000)	0.250	-
Johansson et al. [30] (Re=45000)	0.270	-
Srikanth et al. [32] (Re=150	0.221	1.930
De and Dalal [33] (Re=150)	0.225	1.960
Turner et al. [34] (Re=10000)	0.228	-
Zeitoun et al. [35] (Re=180)	0,201	1.934

The closest result to the experimental one was obtained with using LES turbulence model in terms of flow characteristics and when the results were also compared with literature. The each value of time-averaged pressure coefficient and drag coefficient were closer for k-ε and k-ω turbulence models. While Reynolds number increased to Re=11600, the pressure coefficient becomes lower and the drag coefficient values is also reduced. The results of LES turbulence model were different from other turbulence models. Moreover, the drag coefficient was obtained as C_D=1.179 and 1.141 for k-ε turbulence model at Re=5800 and 11600, respectively. The results of LES turbulence model were different from other turbulence models and its 1.467 at Re=5800 and 1.441 at Re=11600, which is a close agreement with literature. For this reason, LES turbulence model is more convenient for detailed engineering applications around bluff body in absence of experimental data. On the other hand, LES turbulence models require more computer capacities and much solution time. Hence, for the basic applications, k-ε and k-ω turbulence models can also be used.

4. Conclusion

In this study, vortex shedding frequency and flow characteristics such as time-averaged vector field, streamline topology, vorticity, velocity component contours and root mean square (rms) variation depending on the Reynolds numbers at Re=5800 and Re=11600 were investigated by means of time-resolved

PIV and CFD with three different Turbulence Models. In generally, sharp-tip corner of the triangle cross-section cylinder is exposed to free stream flow while the other two sharp-tip corners are placed to the downstream side to form powerful, stable and continuous vortex shedding. The experimental studies are performed in an open water channel by PIV method at Selcuk University of Advanced Technology Research and Application Center in Konya, Turkey. The obtained data were used to validate numerical results. The experimental results are compared to the numerical results obtained by means of transient simulations with RANS (k-ε and k-ω methods) and LES turbulence models of ANSYS-Fluent Software. It is seen that the RANS methods does not give comparable results with the PIV when compared to LES method for the flow structure and force coefficients.

Time averaged flow structure form a mirror appearance both upper and lower section of the symmetry axis of the triangular cylinder in the downstream of the wake region. It is shown from cross comparison flow characteristics that the wake region size is shorter and narrower at Re=11600 than Re=5800 for both experimental and numerical results.From experimental results, two symmetrical foci were formed at the trailing edge with the length of $1.8 < x/L < 1.9$ and $1.6 < x/L < 1.7$ at Re=5800 and 11600, respectively. When the numerical results with the experimental results were compared, the method using LES turbulence model gave the more similar flow field than k-epsilon and k-omega for both Reynolds numbers. In the x-direction, the length of the foci was longer at k-ω turbulence model than the other turbulence models and experimental study for both Reynolds numbers. However, in the y direction, the length of foci was the largest at Re=5800 for k-ε turbulence model which was the second largest at Re=11600.

In addition, Strouhal number (St), pressure coefficients (C_p) and drag coefficients (C_D) were investigated. Using LES method, and the average drag coefficient was found to be C_D=1.467 and C_D=1.441 for Re=5800 and Re=11600 and which was very close to the literature. Closer results for Strouhal number to the literature was found approximately 0.22 using LES method. However, as there are no force and pressure measurement systems in experimental setup, the pressure and drag coefficients were limited to be obtained only with numerical analysis.

Finally, it can be interpreted that the closest results to the experimental results were obtained with using LES turbulence model in terms of flow field and when results were also compared with literature. The difference between the principal flow characteristics obtained with the PIV and LES models was quite acceptable and did not exceed 10%. LES turbulence model is more convenient for detailed engineering applications around bluff body in absence of the experimental data. In future, force and pressure measurement around the body might be performed and compared with the CFD results.

Acknowledgment: The author would like to acknowledge DPT project of Selcuk University's Advanced Research Center Contract No.: 2009K12180. The authors acknowledge the financial support of Selcuk University's Scientific Research Project Office Contract no: 11401058 and 11401059.

References

[1] Amit D and Radhe S (2011) Unsteady Heat Transfer from an Equilateral Triangular Cylinder in the Unconfined Flow Regime, International Scholary Research Network Mechanical Engineering, vol. 2011, pp 776-789, doi: 10.5402/20011/932738.

[2] Xing Z and Blair P (2000) Turbulent vortex shedding from triangular cylinder using the turbulent body force potential model. In: ASME 2000 Fluids Engineering Division Summer Meeting.

[3] Ozgoren M (2006) Flow structure ın the downstream of square and circular cylinders, Flow Measurement and Instrumentation, vol.17, pp 225-235, doi:10.1016/j.flowmeasinst.2005.11.005.

[4] Okajima A (1982) Strouhal numbers of rectangular cylinders, Journal Fluid Mechanics, vol. 123, pp 379-398, doi: 10.1017/S0022112082003115.

[5] Ozgoren M (2013) Flow structures around an equilateral triangle arrangement of three spheres International Journal of Multiphase Flow, vol. 53, pp 54–64, doi:

org/10.1016/j.ijmultiphaseflow.2013.02.001.

[6] Wei-Xi H and HyungJ S (2007), Vortex shedding from a circular cylinder near a moving Wall, Journal of Fluids and Structures, vol. 7, pp1064–1076,doi:10.1016/j.jfluidstructs.2007.02.004.

[7] Hatef A K and Andersson, H.I, (2011) On vortex shedding from a hexagonal cylinder, Physics Letters A , vol.375,pp 4007–4021,doi:10.1016/j.physleta.2011.09.046.

[8] KnaussD T, JohnJ E A and Marks, C H (2012) The vortex frequencies of bluff cylinders at low Reynolds numbers, AIAA J. Hydronautics vol.10, pp 121-126, doi: 10.2514/3.48149.

[9] Liu LS, Ying ZL, Hyung J.S. (2010) On the wake with and without vortex shedding suppression behind a two-dimensional square cylinder in proximity to a plane Wall, J. Wind Eng. Ind. Aerodyn.,vol.98, pp 492–503, doi:10.1016/j.jweia.2010.03.002.

[10] Shun CY and Chen WY (2011) Flow patterns and vortex shedding behavior behind a square cylinder, J. Wind Eng. Ind. Aerodyn.,vol.99, pp 868–878, doi:10.1016/j.jweia.2011.06.006.

[11] Bouris D and Bergeles G (1999) 2D LES of vortex shedding from a square cylinder, Journal of Wind Engineering and Industrial Aerodynamics,vol.80, pp 31-46, doi:10.1016/S0167-6105(98)00200-1.

[12] Huanga R F, Lina B H and Yen S.C, (2010) Time-averaged topological flow patterns and their influence on vortex shedding of a square cylinder in cross-flow at incidence, Journal of Fluids and Structures, vol. 26, pp 406–429, doi:10.1016/j.jfluidstructs.2010.01.003.

[13] Gu F, Wangb J.S, Qiao X Q and Huang Z(2012) Pressure distribution, fluctuating forces and vortex shedding behavior of circular cylinder with rotatable splitter plates, Journal of Fluids and Structures, vol. 28, pp 263–278, doi:10.1016/j.jfluidstructs.2011.11.005.

[14] Sang J L and Jung Y L (2008) PIV measurements of the wake behind a rotationally oscillating circular cylinder, Journal of Fluids and Structures, vol.24, pp 2–17, doi:10.1016/j.jfluidstructs.2007.06.001.

[15] Lam K.M. (2009) Vortex shedding flow behind a slowly rotating circular cylinder, Journal of Fluids and Structures, vol. 25, pp 245–262, doi:10.1016/j.jfluidstructs.2008.04.005.

[16] Kalmbach A and Breuern M (2013) Experimental PIV/V3V measurements of vortex-induced fluid structure interaction in turbulent flow—A new benchmark FSI-PfS-2a , Journal of Fluids and Structures, vol. 42, pp 369–387, doi:10.1016/j.jfluidstructs.2013.07.004.

[17] Cheng M and Liu G.R (2000) Effects of after body shape on flow around prismatic cylinders, Journal of Wind Engineering and Industrial Aerodynamics, vol.84, pp 181-196, doi: 10.1016/S0167-6105(99)00050-1.

[18] Dhiman A and Shyam R (2011) Unsteady Heat Transfer from an Equilateral Triangular Cylinder in the Unconfined Flow Regime, International Scholarly Research Network ISRN Mechanical Engineering Volume, Article ID 932738, 13 pages doi:10.5402/2011/932738.

[19] Saad El-Sherbiny (1983) Flow separation and reattachment over the sides of a 90^{o} triangular prism, J. Wind Eng. Ind. Aerodyn., vol. 11, pp 393-403, doi:10.1016/0167-6105(83)90116-2.

[20] Nakagawa T (1989) Vortex shedding mechanism from a triangular prism in a subsonic flow, Fluid Dyn. Res., vol.5, pp 69-81, doi:10.1016/0169-5983(89)90012-9.

[21] Tatsuno M, Takayama T, Amamoto H and Ishi-I K (1990) On the stable posture of a triangular or a square cylinder about its central axis in a uniform flow, Fluid Dynamics Research, vol. 6, pp 201-207, doi: 10.1016/0169-5983(90)90062-4.

[22] El-Wahed A K , Johnson M W, Sproston J L (1993) Numerical study of vortex shedding from different shaped bluff bodies, Flow Meas. Instrum. vol 4, pp 233-240, doi:10.1016/0955-5986(93)90030-M.

[23] Sharif M A R, Gu Z (2002) Turbulent flow simulation behind a V-shaped flame stabilizer using a nonlinear k-ε model and a smoothing algorithm, Chem. Eng. Communications, vol.189, pp 471-488, doi:10.1080/00986440212092.

[24] Camarri S, Salvetti M V, Buresti G (2006) Large-eddy simulation of the flow around a triangular prism with moderate aspect ratio, Journal of Wind Engineering and Industrial Aerodynamics. vol. 94, pp 309-322, doi:10.1016/j.jweia.2006.01.003.

[25] Chattopadhyay H (2007) Augmentation of heat transfer in a channel using a triangular prism, Int. J. Thermal Sciences, vol. 46, pp 501-505, doi:10.1016/j.ijthermalsci.2006.07.003.

[26] Peng J, Fu X, Chen Y (2008) Experimental investigations of Strouhal number for flows past dual triangulate bluff bodies, Flow Measurement Instrumentation, vol. 19, pp 350-357, doi: 10.1016/j.flowmeasinst.2008.05.002.

[27] Srigrarom S, Koh A K G (2008) Flow field of self-excited rotationally oscillating equilateral triangular cylinder, J. Fluids Struct., vol. 24, pp 750-755, doi:10.1016/j.jfluidstructs.2007.10.015.

[28] Dmitry A L, Ivar S E, Kjell E R (2013) Modeling of turbulent separated flows using OpenFOAM, Computers & Fluids, vol. 80, pp 408–422, doi:10.1016/j.compfluid.2012.01.015.

[29] Hasse C, Sohm V, Wetzel M, Durst B. Hybrid (2009) URANS/LES turbulence simulation of vortex shedding behind a triangular flame holder. J Flow Turbul Combust, vol83, pp 1–20, doi: 10.1007/s10494-008-9186-7.

[30] Johansson S, Davidson L, Olsson E. (1993) Numerical simulation of vortex shedding past triangular cylinders at high Reynolds number using a k-ε turbulence model. Int. J. Numer. Methods Fluids 16, 859–878.

[31] Sjunnesson A, Nelsson C, Erland M. (1991) LDA measurements of velocities and turbulence in a bluff body stabilized flame. Tech. rep., Volvo Flygmotor AB, Trollhättan, Sweden.

[32] Srikanth S, Dhiman A K, Bijjam S (2010)Confined flow and heat transfer across a triangular cylinder in a channel, International Journal of Thermal Sciences, vol. 49, pp 2191-2200, doi:10.1016/j.ijthermalsci.2010.06.010.

[33] De A K and Dalal A (2006) Numerical Study of Laminar Forced Convection Fluid Flow and Heat Transfer From a Triangular Cylinder Placed in a Channel, J. Heat Transfer, vol. 129(5), pp 646-656, doi:10.1115/1.2712848.

[34] Turner J T, Popiel C O, Robinson D I (1993) Evolution of an improved vortex generator, Flow Measurement and Instrumentation, vol. 4, pp 249–258, doi:10.1016/0955-5986(93)90032-E.

[35] Zeitoun O, Mohamed A, Nuhait A (2011) Convective heat transfer around a triangular cylinder in an air cross flow, International Journal of Thermal Sciences, vol. 50, pp 1685-1697, doi:10.1016/j.ijthermalsci.2011.04.011.

[36] Stefan H J, Davidson L and Olsson E (1993) Numerical simulation of vortex shedding past triangular cylinders at high Reynolds number using a *k*-ε turbulence model, International Journal for Numerical Methods in Fluids, vol.16, pp 859–878, doi: 10.1002/fld.1650161002.

[37] Lun Y F, Mochida A, Murakami S, Yoshino H and Shirasawa T (2003) Numerical simulation of flow over topographic features by revised *k–ε* models, Journal of Wind Engineering and Industrial Aerodynamics, vol. 91, pp 231-245, doi:10.1016/S0167-6105(02)00348-3.

[38] Shome B (2013) Numerical study of oscillating boundary layer flow over a flat plate using$k–k_L–\omega$ turbulence model, International Journal of Heat and Fluid Flow, vol. 42, pp 131-138, doi:10.1016/j.ijheatfluidflow.2013.03.002.

[39] Kim S, Wilson P A and Chen Z M (2015) Effect of turbulence modelling on 3-D LES of transitional flow behind a circular cylinder, Ocean Engineering, vol. 100, pp 19-25, doi:10.1016/j.oceaneng.2015.03.014.

[40] Anonymous, Fluent 14.0 User Guide, Fluent Inc. 2013.